

DRAFT: October 31, 2018

# On the Origin of the High-Ionization Intermediate-Velocity Gas Toward HD 14434<sup>1</sup>

David C. Knauth<sup>2</sup>, J. Christopher Howk<sup>2,3</sup>, Kenneth R. Sembach<sup>4</sup>, James T. Lauroesch<sup>5</sup>,  
and David M. Meyer<sup>5</sup>

## ABSTRACT

We present *Far Ultraviolet Spectroscopic Explorer* and Space Telescope Imaging Spectrograph observations of high-ionization interstellar absorption toward HD 14434  $[(l, b) = (135^\circ.1, -3^\circ.8); d \sim 2.3 \text{ kpc}]$ , an O5.5 V star in the Perseus OB1 Association. Intermediate-velocity interstellar Si IV and C IV absorption is present at  $V_{LSR} = -67 \text{ km s}^{-1}$ , while low-ionization gas associated with the Perseus arm is detected at  $\sim -50 \text{ km s}^{-1}$ . Neither N V nor O VI is detected at  $V_{LSR} = -67 \text{ km s}^{-1}$ ; although Al III and Fe III, tracers of warm ionized gas, are seen. The high-ion column densities in the  $-67 \text{ km s}^{-1}$  component are  $\log[N(\text{C IV})] = 13.92 \pm 0.02 \text{ cm}^{-2}$ ,  $\log[N(\text{Si IV})] = 13.34 \pm 0.02 \text{ cm}^{-2}$ ,  $\log[N(\text{N V})] \leq 12.65 \text{ cm}^{-2}$ , and  $\log[N(\text{O VI})] \leq 13.73 \text{ cm}^{-2}$  ( $3\text{-}\sigma$  limits). The observed C IV/Si IV ratio of  $3.8 \pm 0.3$  in this intermediate-velocity cloud (IVC) is similar to the Galactic average ( $4.3 \pm 1.9$ ). Our analysis of the Si IV and C IV line widths yields a temperature of  $T \sim 10,450 \pm 3,400 \text{ K}$  for this component. At this low temperature, neither Si IV nor C IV can be produced via collisions. We investigate several photoionization models to explain the intermediate-velocity

---

<sup>1</sup>Based on observations made with the NASA/ESA Hubble Space Telescope, obtained from the data archive at the Space Telescope Science Institute. STScI is operated by the Association of Universities for Research in Astronomy, Inc. under the NASA contract NAS 5-26555.

<sup>2</sup>*FUSE* Science Center, Department of Physics and Astronomy, The Johns Hopkins University, Baltimore, MD 21218; dknauth@pha.jhu.edu.

<sup>3</sup>Current address: Center for Astrophysics and Space Sciences, University of California at San Diego, C-0424, La Jolla, CA, 92093; howk@tralfalgar.ucsd.edu.

<sup>4</sup>Space Telescope Science Institute, 3700 San Martin Dr., Baltimore, MD 21218; sembach@stsci.edu.

<sup>5</sup>Department of Physics and Astronomy, Dearborn Observatory, 2131 Sheridan Road, Northwestern University, Evanston, IL 60208; jtl@elvis.astro.nwu.edu; davemeyer@northwestern.edu.

Si IV and C IV absorption toward HD 14434. Photoionization models employing cooling of a hot ( $T \sim 10^6$  K) diffuse plasma as the source of ionizing radiation reproduces the observed properties of the IVC toward HD 14434 quite well. The hot plasma responsible for the ionizing radiation in these models may be attributed to hot gas contained in a supershell in or near the Perseus Arm or from a more generally distributed hot ionized medium.

*Subject headings:* ISM: atoms — ISM: abundances — ISM: clouds — ISM: structure — Stars: individual (HD 14434) — Galaxy: kinematics and dynamics — Galaxy: open clusters and associations: individual (Per OB1) — ultraviolet: ISM

## 1. Introduction

The canonical picture of the interstellar medium (ISM) in the Galactic disk is one in which the gas resides in multiple “phases” in rough pressure equilibrium with one another. While the details vary (Cox & Smith 1974; McKee & Ostriker 1977), all global models of the ISM in the Milky Way include a hot component ( $T \sim 10^5$  to  $> 10^6$  K). This hot component, motivated by the detection of Li-like oxygen (O VI) absorption (Rogerson et al. 1973) and X-ray emission (Williamson et al. 1974) from the ISM some 30 years ago, is maintained by the input of energy and matter from massive stars into the ISM through stellar winds and supernovae. The precise nature of this feedback into the ISM is not well understood, although it is thought to provide for, among other things, the energy required to explain the quantity and distribution of the “high-ions” O VI, N V, C IV, and Si IV in the Milky Way (e.g., Savage, Sembach, & Lu 1997; Savage et al. 2002).

OB associations containing young, massive stars are ideal locations for studying the hot interstellar medium, since these stars are believed to be directly responsible for its production. The massive Perseus OB1 Association resides in the Perseus Arm of the Milky Way, some 2.3 kpc from the Sun (Garmany & Stencel 1992). The *International Ultraviolet Explorer (IUE)* detected high-velocity absorption in the highly-ionized species Al III, Si IV, and C IV toward several stars in this association (Phillips & Gondhalekar 1981; McLachlan & Nandy 1985; Savage, Meade, & Sembach 2001). Phillips & Gondhalekar (1981) and McLachlan & Nandy (1985) concluded that this highly-ionized gas was caused by a supernova explosion within Per OB1 itself. This region is rife with evidence of stellar feedback on massive scales, including the presence of H I and H $\alpha$  supershells (Heiles 1979; Reynolds, Sterling, & Haffner 2001; Madsen, Haffner, & Reynolds 2002), lending indirect support to their conclusion. However, the physical processes directly responsible for the production of the observed highly-ionized gas are unconstrained.

In this work, we focus on the ionized gas observed toward HD 14434, a member of the Perseus OB1 Association. High-resolution Space Telescope Imaging Spectrograph (STIS) and *Far Ultraviolet Spectroscopic Explorer* (*FUSE*) observations of interstellar absorption associated with the Perseus Arm toward HD 14434 are presented. This sight line is remarkable for the presence of an intermediate-velocity cloud (IVC), the velocity of which is inconsistent with its origin in the quiescent gas of the Perseus Arm. This cloud is seen strongly in the highly-ionized species Si IV and C IV; it shows some absorption from the moderately-ionized species Al III and Fe III and none from the more highly-ionized species N V and O VI. While this cloud was seen with *IUE*, the echelle-mode STIS observations presented here constrain its temperature to a range that is indicative of photoionized material, and we will show that this material is likely ionized by emission from a diffuse X-ray emitting hot plasma.

This paper is organized as follows. A description of the HD14434 sight line is given in §2. The STIS and *FUSE* observations and data reduction techniques are described in §3. In §4, the absorption line measurements are discussed. The nature of the highly-ionized gas toward HD 14434 is presented in §5. Our conclusions are summarized in §6.

## 2. The Sight Line toward HD 14434

HD 14434, an O5.5 Vnfp star (Walborn 1972), is a member of the Per OB1 Association, which is a region of active star formation. Table 1 contains the relevant stellar parameters used throughout this work. We assume the distance to HD 14434 is 2.3 kpc, the distance to Per OB1 (Garmany & Stencel 1992). At this distance the line of sight toward HD 14434 passes through both the Local Arm ( $V_{LSR} \sim 0 \text{ km s}^{-1}$ ) and the Perseus Arm ( $V_{LSR} \sim -50 \text{ km s}^{-1}$ ). Figure 1 shows the 21cm H I emission results of the Ledien/Dwingeloo Survey (Hartmann & Burton 1997) and H $\alpha$  emission obtained by WHAM, the Wisconsin H $\alpha$  Mapper, (Haffner et al. 2001) toward HD 14434. The 21cm H I data clearly reveal two components from the Local and Perseus Arms and a single weak component associated with the Outer Arm ( $V_{lsr} = -100 \text{ km s}^{-1}$ ). The H $\alpha$  data show a single broad component centered at  $V_{lsr} = -25 \text{ km s}^{-1}$ . At  $V_{lsr} = -67 \text{ km s}^{-1}$  (vertical line in Figure 1), the velocity of the IVC studied here, neither H I nor H $\alpha$  reveal any clues as to the presence of the IVC.

Evidence for star-ISM interaction is prevalent in this region. In addition to being an active star forming region, Per OB1 resides in close proximity to the double cluster  $h$  and  $\chi$  Per [NGC 869 at  $(l, b) = (134^\circ.5, -3^\circ.5)$  and NGC 884 at  $(l, b) = (135^\circ.1, -3^\circ.6)$ ]. These open clusters are believed to be related to Per OB1, with evidence for three episodes of star formation in this localized region of the Perseus Arm (Schild 1967; Marco & Bernabeu 2001).

High-resolution H I observations show the presence of numerous wind-blown interstellar bubbles around many stars in this region (Cappa & Herbstmeier 2000), including HD 13022, HD 13338, HD 14442, and HD 14947, all members of Per OB1. Additionally, Heiles (1979) has identified two Galactic supershells in the vicinity of Per OB1: GS139-03-69 at  $l = 139^\circ$  and  $b = -3^\circ$  with  $\Delta l = 18^\circ$  and  $\Delta b = 10^\circ$ , and one unnamed shell  $5^\circ$  in diameter centered on Per OB1 at  $l = 135^\circ$  and  $b = -4^\circ$  (Heiles 1979). Following Heiles’s naming convention, we refer to this shell as GS135-04-27. The GS139-03-69 supershell is visible in the velocity range  $-87 \leq V_{LSR} \leq -59 \text{ km s}^{-1}$  (Heiles 1979; Knee & Brunt 2001), while the observed velocity range for GS135-04-27 is  $-31 \leq V_{LSR} \leq -23 \text{ km s}^{-1}$  (Heiles 1979). The H I emission detected between  $-60$  and  $-70 \text{ km s}^{-1}$  in the vicinity around  $(l, b) \sim (135^\circ, -3^\circ 5')$  is likely associated with the southern rim of the GS139-03-69 (Knee 2003, private communication). However, the standard Galactic rotation model predicts a distance to GS139-03-069 of 9 kpc (Kerr & Lynden-Bell 1986) much further away than Per OB2. It is important to note that an accurate distance cannot be obtained from velocity information alone, therefore an association between GS139-03-69 and our IVC cannot be ruled out. Higher spatial resolution H I and H $\alpha$  data toward HD 14434 and Per OB2 are required to obtain further insight.

Recent observations from the Wisconsin H $\alpha$  Mapper (WHAM) detect a supershell-like structure in the velocity range  $-60 \text{ km s}^{-1} \leq V_{LSR} \leq -40 \text{ km s}^{-1}$  approximately centered on Per OB1 (Madsen, Haffner, & Reynolds 2002). This velocity range is similar to that seen in intermediate and high-ion absorption (Philips & Gondhalekar 1981; McLachlan & Nandy 1985; this work). The extended structure seen south of the plane in the Perseus Arm may be related to the northern supershell studied by Reynolds, Sterling, & Haffner (2001).

The large-scale structures identified in H I and H $\alpha$  emission are likely related to the vigorous star formation occurring in the Galactic disk near this region. In particular, the W4 H II region is found at  $(l, b) = (134^\circ 7', 0^\circ 9')$ , and there is a large amount of evidence that the stars in this region are influencing the ISM on large scales (Normandeau, Taylor, & Dewdney 1996). Star formation associated with W4 may be responsible for driving the vertically-extended structures seen in the H $\alpha$  maps of Reynolds et al. (2001) and Madsen et al. (2002). While the observations summarized above are not focused on the specific sight line toward HD 14434, it is important to note that the region in which HD 14434 resides is strongly affected by the presence of massive stars.

### 3. Observations and Data Reduction

#### 3.1. STIS

HD 14434 was observed on 2001 April 6, by STIS onboard the *Hubble Space Telescope* (*HST*) as part of the guest observer proposal “Snapshot Survey of the Hot ISM” (ID 8662). The data were acquired with the E140M grating and the  $0.2'' \times 0.2''$  aperture for a total exposure time of 1440 seconds. This setup provides 43 echelle orders covering the complete wavelength range from  $1150 - 1725 \text{ \AA}$  at a resolving power of  $R \sim 46,000$  ( $\Delta v = 6.5 \text{ km s}^{-1}$ ). There are two pixels per resolution element. The data were reduced and extracted with the CALSTIS pipeline (v2.11). The subtraction of background and scattered light from these echelle data employs the algorithm of Lindler & Bowyers (2000). CALSTIS provides the appropriate Doppler correction to remove the effect of the spacecraft motion and places the spectra on the heliocentric velocity scale ( $V_{helio}$ ), accurate to  $0.8\text{--}1.6 \text{ km s}^{-1}$ . An additional shift of  $+3 \text{ km s}^{-1}$  is required to shift the data from the  $V_{helio}$  to that of the Local Standard of Rest,  $V_{LSR}$ .<sup>6</sup> The final spectrum has a signal-to-noise (S/N) ratio of  $\sim 40$  per resolution element at  $1240 \text{ \AA}$ . Further information on the design and performance of STIS can be found in Woodgate et al. (1998) and Kimble et al. (1998).

#### 3.2. FUSE

Two exposures of HD 14434 were obtained by *FUSE* on 1999 November 24 for a total exposure time of 4441 seconds (archival IDs P1020504001-002). The data, which cover the wavelength range  $905 - 1185 \text{ \AA}$ , were acquired with the star in the center of the large ( $30'' \times 30''$ ) aperture and resulted in high resolution ( $\Delta v \sim 20 \text{ km s}^{-1}$ ) spectra. The alignment of the four channels was well maintained during both exposures. Only data from the LiF1 channel are presented here since this channel has the highest sensitivity. (This is the channel used for guiding.) We utilized the other three channels to provide a consistency check to rule out the possibility of detector artifacts. We refer the reader to Moos et al. (2000) and Sahnou et al. (2000) for more detailed discussions of *FUSE* and its on-orbit performance.

The time-tagged data were reduced and calibrated with CalFUSE<sup>7</sup> (version 1.8.7 Dixon et al. 2001) the standard *FUSE* pipeline processing software. The data were co-added with

---

<sup>6</sup>We adopt the standard *IAU* definition of the LSR, assuming a Solar motion of  $+20 \text{ km s}^{-1}$  in the direction  $(\alpha, \delta)_{1900} = (18^h, +30^\circ)$  [ $(l, b) \approx (56^\circ, +23^\circ)$ ], which gives  $V_{LSR} = V_{helio} + 3 \text{ km s}^{-1}$  in the direction of HD 14434.

<sup>7</sup>The CalFUSE pipeline reference guide is available at [http://fuse.pha.jhu.edu/analysis/pipeline\\_reference.html](http://fuse.pha.jhu.edu/analysis/pipeline_reference.html).

a cross-correlation technique in order to minimize uncertainties in the relative wavelength calibration in each spectrum. The wavelength solution used provides good relative calibration across the LiF channels. Relative wavelength calibration errors for *FUSE* data calibrated with CalFUSE v1.8.7 are equivalent to  $\sim \pm 6\text{-}10 \text{ km s}^{-1}$  ( $1\text{-}\sigma$ ). The absolute wavelength scale of *FUSE* is not well constrained. We used interstellar Fe II lines in the STIS and *FUSE* spectra to fix the *FUSE* velocity scale to the STIS  $V_{LSR}$  scale. The final summed LiF1A spectrum (near 1050 Å) and the LiF1B spectrum (near 1140 Å) have S/N ratios of  $\sim 20$  and  $\sim 32$  per resolution element, respectively. The uncertainties used in calculating the S/N ratios include a significant contribution from fixed-pattern noise.

#### 4. Analysis and Results

In our measurements all stellar continua were modeled with low order Legendre polynomials (order  $\leq 4$ ), with the exception of the O VI lines (described below). Figure 2 shows normalized absorption profiles of several low-ionization species (Al II, Mg II, Fe II, and Fe III) as well as profiles of the high-ionization species (Si IV, C IV, N V, and O VI), which are the main focus of this work. As seen from Figure 2, no detection of either N V or O VI is evident, while C IV and Si IV are detected only at the velocity of the IVC. The lower ionization species (e.g., Fe II and Mg II) are detected primarily in the Local and Perseus Arm material. The Perseus Arm component of Al III from *IUE* (Savage, Meade, & Sembach 2001) and Fe III is blended with the IVC gas. It is interesting to note that no C IV or Si IV absorption is detected at the velocity of the Local or Perseus Arms suggesting that different physical conditions exist for the IVC gas. We hypothesize that the blue-shifted high-ionization IVC is material once associated with the Perseus Arm which has been accelerated.

We use the procedures outlined by Sembach & Savage (1992) for measuring equivalent widths of the Perseus Arm absorption and estimating the errors in the measurements. These are given in Table 2, along with an equivalent width weighted average velocity. With the exception of Al III (Savage, Meade, & Sembach 2001), all measurements are from this work. The velocities and column densities measurements agree well from the independent fits from two or more lines for each species, except Fe III. The difference in velocities for the two Al III lines is due to the poor quality of the *IUE* data (Savage, Meade, & Sembach 2001). The quoted  $1\text{-}\sigma$  uncertainties include contributions from statistical uncertainties, fluctuations due to fixed pattern noise, and definable continuum placement errors that were added in quadrature. No systematic continuum placement uncertainties were included in the error budget. Uncertainties for the STIS data are dominated by statistical and continuum placement uncertainties as the contribution from fixed-pattern noise is small. When no detection

was evident,  $3\text{-}\sigma$  upper limits are presented following the prescription of Morton, York, & Jenkins (1986).

#### 4.1. O VI Concerns

The region around O VI  $\lambda 1031.926$ , shown in the bottom panel of Figure 3, is complicated by the presence of O VI in the outflowing stellar wind, H I Ly- $\beta$  absorption at  $1025.723 \text{ \AA}$ , and H<sub>2</sub> 6–0 P(3) and R(4) absorption at  $1031.191 \text{ \AA}$  and  $1032.356 \text{ \AA}$ . The weaker member of the O VI doublet at  $1037.617 \text{ \AA}$  is not used in the analysis due to the severe blending with C II\* at  $1037.018 \text{ \AA}$  and the strong H<sub>2</sub> 5–0 R(1) and P(1) absorption at  $1037.146 \text{ \AA}$  and  $1038.156 \text{ \AA}$ . The stronger member of the O VI doublet may also be contaminated by HD 6–0 R(0) absorption at  $1031.912 \text{ \AA}$  (Sembach 1999) along sight lines with substantial H<sub>2</sub> [ $\log N(\text{H}_2) \geq 19$ ]. Careful examination of the entire LiF1A spectrum reveals the presence of several unblended HD lines arising from gas in the Local Arm (though none are detected in the Perseus Arm gas). We applied a curve of growth analysis (see below) for five unblended HD lines and determined the equivalent width ( $W_\lambda$ ) of the contaminating HD line to be  $58.0 \text{ m\AA}$ . A simple Gaussian model of the HD contamination was generated and divided into the normalized O VI profile to produce the final unblended O VI spectrum.

The continuum placement of the stronger interstellar O VI line is potentially affected by the presence of a stellar wind feature in the weaker O VI line. This feature is not detected in the stronger O VI line due to its overlap with H I Ly- $\beta$ . Figure 3 shows the stellar wind profiles of Si IV  $\lambda 1393.755$ , C IV  $\lambda 1548.195$ , N V  $\lambda 1238.821$ , and O VI  $\lambda 1031.926$ . A stellar wind feature is clearly observed in Si IV over the range  $-2100 \text{ km s}^{-1} \leq v \leq -1700 \text{ km s}^{-1}$  (see top panel of Figure 3), close to the terminal velocity of  $V_\infty = 2120 \pm 20 \text{ km s}^{-1}$  (this work), which is  $\sim 200 \text{ km s}^{-1}$  greater than that derived by Howarth & Prinja (1989) based on *IUE* data. The terminal wind velocity is determined from the short wavelength absorption limit of the P Cygni C IV wind line at  $1548 \text{ \AA}$ . This wind feature cannot be seen in either the C IV or N V winds because they are saturated (see middle two panels of Figure 3). The wind feature coincides in velocity space with a broad depression near the interstellar O VI line (demarcated by the vertical dashed lines in Figure 3). Though the STIS and *FUSE* data were acquired about two years apart, stellar wind features that occur at or near the terminal velocity, as is the case here, are typically long-lasting entities (A. Fullerton 2002, private communication). These factors indicate that the broad absorption coincident with the interstellar O VI  $1032 \text{ \AA}$  absorption could be due to structure in the outflowing wind of the star. Due to the uncertainties in modelling the stellar continuum in the region surrounding the O VI  $1032 \text{ \AA}$  absorption, we give a conservative upper limit to

$N(\text{O VI})$  in Table 2.

## 4.2. Apparent Optical Depth Method

A useful tool for determining the column density of an absorbing species is the apparent optical depth method (Savage & Sembach 1991). The apparent optical depth,  $\tau_a(v)$ , is a valid, instrumentally-blurred representation of the true optical depth in the absence of unresolved saturated structure within the line profile. The continuum normalized absorption line profile,  $I(v) \equiv e^{-\tau_a(v)}$ , is related to apparent column density per unit velocity,  $N_a(v)$ , by

$$N_a(v) = \frac{m_e c}{\pi e^2} \frac{\tau_a(v)}{f \lambda} = 3.768 \times 10^{14} \frac{\tau_a(v)}{f \lambda(\text{\AA})} \text{ ions cm}^{-2} (\text{km s}^{-1})^{-1}. \quad (1)$$

In this equation,  $m_e$  and  $e$  denote the mass and charge of the electron, respectively,  $c$  is the speed of light,  $f$  is the atomic oscillator strength, and  $\lambda$  is the laboratory wavelength of the transition. Savage & Sembach (1991) showed that  $N_a(v)$  is equivalent to the true column density as a function of velocity,  $N(v)$ , if there is no unresolved saturated structure. The presence of unresolved saturated structure can be identified through the comparison of  $N_a(v)$  profiles for different transitions of the same species with differing  $f$ -values. In situations where unresolved saturation is present, the derived  $N_a(v)$  is always a lower limit to the true column density. The integrated apparent column densities are listed in Table 2.

The  $N_a(v)$  profiles for both members of the Si IV and C IV doublets are shown in the top and middle panels, respectively, of Figure 4. In each case the stronger line is denoted by the solid circles, while the weaker line is represented by the open squares. The overall agreement between the  $N_a(v)$  profiles for both members of the Si IV and C IV doublets implies little or no evidence for saturation, and hence  $N_a(v) = N(v)$ . The bottom panel of Figure 4 shows a comparison of the weaker members of the Si IV and C IV doublets along the line of sight toward HD 14434. There is an excellent correspondence between the Si IV and C IV profiles over the entire velocity extent of the lines. This similarity suggests that Si IV and C IV arise in the same gas (i.e., they are co-spatial). In addition, the similar line widths indicate that the dominant broadening mechanism is non-thermal (e.g., turbulence). The derived C IV/Si IV ratio is  $3.8 \pm 0.3$ , quite similar to the Galactic average of  $4.3 \pm 1.9$  (Sembach, Savage, & Tripp 1997).

As a check on the apparent optical depth method, we performed curve of growth (COG) analyses for HD and Fe II. All HD lines are on the flat part of the curve of growth and no HD column density was obtained. The COG for Fe II yielded  $\log[N(\text{Fe II})] = 14.90 \pm 0.06$

$\text{cm}^{-2}$  and a  $b$ -value of  $23.0 \pm 4.4 \text{ km s}^{-1}$ ; the large  $b$ -value is due to the contribution of both IVC and Perseus Arm material. This column density is in good agreement with that determined from the apparent optical depth method, therefore Fe II is unsaturated. The unsaturated Fe II lines (see Table 2) probe a larger apparent optical depth ( $\tau_a \leq 3$ ) than does Fe III  $\lambda 1122.546$  ( $\tau_a \leq 1$ ). Subsequently, we assume that Fe III is unsaturated. We adopt the curve of growth results for the Fe II and the apparent column density results for the Mg II, Fe III, Si IV, and C IV. The final adopted columns are presented in Table 4. No results are tabulated for HD due to the fact that all HD lines are on the flat part of the curve of growth.

### 4.3. Component Synthesis

A visual examination of the Si IV and C IV line profiles in Figure 2 reveals a slight asymmetry in the line profiles suggesting the presence of multiple velocity components. We, therefore, used the profile fitting code **Owens.f** developed by Martin Lemoine and the French *FUSE* Team (Lemoine et al. 2002) to fit both one- and two-component model to the data. Because the Si IV and C IV absorption toward HD 14434 are co-spatial, the line profiles of both species were fit simultaneously keeping only the number of velocity components fixed. The free parameters in the profile synthesis are:  $V_{LSR}$ ,  $N(\text{C IV})$ ,  $N(\text{Si IV})$ , nonthermal velocity ( $v_{nt}$ ), and kinetic temperature ( $T$ ). The values of  $v_{nt}$  and  $T$  were obtained from the following definition of the Doppler broadening parameter,  $b^2 = 2kT/Am_H + v_{nt}^2$ , where  $k$  is Boltzmann’s constant,  $A$  is the atomic weight, and  $m_H$  is the mass of a hydrogen atom. The fits are shown in Figure 5 and the results summarized in Table 3. The quoted  $1\text{-}\sigma$  uncertainties do not include systematic errors in the continuum placement, although definable statistical and continuum placement errors are included (see Sembach & Savage 1992).

The best one-component model resulted in a reduced  $\chi^2$  ( $\chi^2/\nu$ ) of 1.42. For this model, a value of  $v_{nt} = 12.0 \pm 0.2 \text{ km s}^{-1}$  and  $T = 10,450 \pm 3,400 \text{ K}$  are derived. For the two-component model, the values of  $v_{nt}$  and  $T$  are  $10.7 \text{ km s}^{-1}$  and  $26,500 \text{ K}$  and  $11.3 \text{ km s}^{-1}$  and  $10,100 \text{ K}$ , for the blue and red velocity components, respectively. The two-component fit resulted in an increased  $\chi^2/\nu$ , compared with the one-component model. The application of an F-test (Lupton 1993) to the model results reveals that the second component is justified at the 30% confidence level. Thus, the evidence for a second component is not statistically significant. Due to its low confidence, no error bars are given for the two component model.

## 5. The Nature of the Highly-Ionized, Intermediate-Velocity Cloud

The strong Si IV and C IV absorption toward HD 14434 is found in a single IVC centered at  $-67 \text{ km s}^{-1}$  that is offset by  $\sim -20 \text{ km s}^{-1}$  from the lower-ionization absorption associated with the Perseus Arm gas (see Figure 2). A profile synthesis analysis shows this highly-ionized IVC is dominated by nonthermal broadening with  $v_{nt} = 12.0 \pm 0.2 \text{ km s}^{-1}$  and is at a relatively cool temperature of  $T = 10,450 \pm 3,400 \text{ K}$ . Our apparent optical depth analysis (see Figure 4) suggests that Si IV and C IV are co-spatial along the line of sight with a C IV/Si IV ratio of  $3.8 \pm 0.3$ , which is consistent with the Galactic average (Savage, Sembach, & Tripp 1997). Our measured ratio is similar to C IV/Si IV  $\sim 3$  found by McLaclan & Nandy (1985) using *IUE* data. They concluded that a supernova explosion was the origin of the intermediate-velocity C IV and Si IV absorption toward Per OB1. However, our derived low temperature does not support this conclusion. Therefore, in this section we discuss the existing models as they apply to the origin of the high-ion intermediate-velocity absorption toward HD 14434.

At a temperature of  $10^4 \text{ K}$ , neither Si IV or C IV would be present if equilibrium collisional ionization prevailed (Sutherland & Dopita 1993). It is generally believed that the presence of Si IV and C IV absorption in the ISM often arises as a result of non-equilibrium collisional ionization at interfaces of hot gas ( $T \sim 10^6 \text{ K}$ ) with relatively cool ( $T \sim 10^2 - 10^4 \text{ K}$ ) interstellar clouds. Spitzer (1996) provides a good, concise review of the existing models. Non-equilibrium collisional ionization, through models of turbulent mixing layers (Slavin, Shull, & Begelman 1993), cooling galactic fountain gas (Shapiro & Benjamin 1992), and conductive interfaces (Ballet, Arnaud, & Rothenflug 1986; Böhringer & Hartquist 1987; Borkowski, Balbus, & Fristrom 1990; Breitschwerdt & Schmutzler 1994), results in gas at  $T \sim 10^5 \text{ K}$  and cannot reproduce the observed C IV/Si IV ratio. Inclusion of self-photoionization (Shapiro & Benjamin 1992; Slavin et al. 1993; Breitschwerdt & Schmutzler 1994) improves the agreement between the observed C IV/Si IV ratio and that predicted by the models. However, these models simultaneously over-produce both N V and O VI by an order of magnitude and have an order of magnitude higher temperature compared with the highly-ionized IVC toward HD 14434. In general, models which rely solely on collisional ionization, including turbulent mixing layers, cooling galactic fountain gas, and conductive interfaces, cannot explain the Si IV or C IV absorption toward HD 14434.

In a time-dependent non-equilibrium model of radiative cooling, Shapiro & Moore (1976) calculated the ionization fraction of several species (H, O, N, C, Si, etc.). In non-equilibrium situations, gas initially at  $T \geq 10^5 \text{ K}$  would cool more rapidly than high-ions recombine leaving the gas “over ionized” for its temperature (Kafatos 1973). Their model follows a parcel of cooling hot gas from an initial temperature of  $10^6 \text{ K}$  to a final temperature of

$10^4$  K. The lower temperature is similar to that derived for the highly-ionized IVC toward HD 14434. The resulting C IV/Si IV and C IV/Fe III ratios predicted by Shapiro & Moore (1976) at  $T \sim 10^4$  K are 1.6 and 7.4. The C IV/Si IV ratio is approximately a factor of 2 too low, while the C IV/Fe III ratio is consistent with the observations. More recently, Edgar & Chevalier (1986) developed a model similar to that of Shapiro & Moore (1976) which included updated atomic data for more species and followed the cooling gas with several assumptions regarding its evolution (e.g., isobaric, isochoric). Their calculations resulted in a C IV/Si IV ratio is a factor of 3 to 10 times larger (depending on the assumptions) than the observed ratio toward HD 14434. Inclusion of self-photoionization may resolve the differences between these models and the observations. Future non-equilibrium calculations which include the effects of self-photoionization are needed to determine if this is a viable mechanism to explain the C IV/Si IV ratio.

Another model which results in the production of Si IV and C IV at relatively cool temperatures is that of wind-blown interstellar bubbles, whose evolution was outlined by Castor, McCray, & Weaver (1975) and Weaver et al. (1977). Stars of spectral type earlier than B2 are known to have strong stellar winds (Howarth & Prinja 1989). The outflowing stellar wind of a star impinges on the ambient ISM and can create an interstellar bubble which have been found to be common around Wolf-Rayet and O-type stars (Chu et al. 1982; Lozinskaya 1991; Cappa & Herbstmeier 2000). The Weaver et al. (1977) model predicts the physical quantities associated with shells driven by the winds from early-type stars including the radius of the shell, expansion velocity, and the column density of O VI and other highly-ionized species. Comparison of the high-ion predictions of the Weaver et al. model<sup>8</sup> with the properties of the highly-ionized IVC toward HD 14434, assuming it is associated with a wind-blown bubble, results in a C IV/Si IV ratio  $\sim 16$  which is a factor of 4 too large. Therefore, we conclude that the presence of a Weaver-type bubble cannot be responsible for the observed highly-ionized IVC toward HD 14434.

The derived temperature ( $T \sim 10^4$  K) and turbulent velocity ( $v_{nt} \sim 12$  km s<sup>-1</sup>) of the IVC are typical of gas found in Galactic H II regions (Reynolds 1991). The low temperature, in particular, suggests that photoionization may play a role in the origin of the high ions toward HD 14434. We used the photoionization equilibrium code Cloudy (v94; Ferland 1996; Ferland et al. 1998) to investigate the possibility that photoionization may explain the observed properties of the IVC seen toward HD 14434. We considered two photoionization scenarios: (i) the IVC is associated with a normal H II region surrounding HD 14434; (ii)

---

<sup>8</sup>We adopt the stellar parameters listed in Table 1 and the following parameters for the model: an ambient interstellar density,  $n_o = 1$  cm<sup>-3</sup>, and a typical age of an interstellar bubble,  $t = 2.3$  Myr (Cappa & Herbstmeier 2000).

the IVC has been ionized by emission from a hot, thermal plasma.

Following Howk & Savage (1999), a suite of single-star H II region models were computed using Cloudy and the stellar parameters in Table 1. For simplicity, we assume that X-rays emitted by the stellar wind can be modelled as an equilibrium plasma at  $T = 10^6$  K with an intensity normalized such that  $L_X/L_{bol} \sim 10^{-7}$  K (e.g., Cassinelli et al. 1981). The results of these models are summarized in Table 5. All the models yield a predicted C IV/Si IV ratio  $\leq 1$ . This ratio could be raised by assuming lower densities, but the lowest density model in Table 5 should already be considered extreme. We note that these models, following Sembach et al. (2000), assume depleted abundances appropriate for the warm neutral medium (WNM) of Galaxy; assuming solar system abundances would lower this ratio. Thus standard H II region models seem unable to explain the observed properties of the gas.

Finally, we investigated the ionization characteristics of a plane-parallel cloud illuminated by emission from a diffuse hot plasma. We assume an ionizing spectrum made up of a diffuse interstellar radiation field (Black 1987) and, following Slavin & Frisch (2002), emission from a thermal plasma. The thermal plasma is chosen to have a temperature of  $\log(T_{\text{plasma}}) = 6.1$  K (Models 1, 2, and 3) or 7.0 K (Model 4). For Models 1, 2, and 4, the flux is normalized to match the observation of the diffuse X-ray background of the Local Bubble. For Model 3, we normalized the emission spectrum to a diffuse X-ray background with a factor-of-10 higher flux. Figure 6 shows the spectrum of ionizing radiation was used as the source of photoionization for our Cloudy Models 1 and 2. We have investigated the use of the Solar System abundances (Model 1; Anders & Grevesse 1989) as well as the depleted abundances characteristics of the WNM<sup>9</sup> described above (Models 2, 3, and 4; following Sembach et al. 2000). We then calculated the combination of total hydrogen density and column density that provided the closest match to the C IV and Si IV column densities seen in the IVC toward HD 14434.

Table 6 summarizes the properties of our photoionization models of a gas cloud illuminated by emission from a cooling hot plasma. All models match the observed C IV/Si IV ratio for reasonable  $N(\text{H})$  of about  $10^{19} \text{ cm}^{-2}$ . The resulting temperatures are within  $2\text{-}\sigma$  of that derived from the Si IV and C IV line widths. Models 1 and 2 predict densities and temperatures of  $n_{\text{H}} = 0.001 \text{ cm}^{-3}$  and  $T = 4,630$  K and  $n_{\text{H}} 0.002 \text{ cm}^{-3}$  and  $T = 6,930$  K, respectively. Increasing the X-ray flux (Model 3) results in  $n_{\text{H}} = 0.016 \text{ cm}^{-3}$  and  $T = 10,100$  K and increasing the temperature of the emitting plasma (Model 4) results in  $n_{\text{H}} = 0.2$

---

<sup>9</sup>The Solar abundance model results in a lower temperature because interstellar grains were not included. A more detailed treatment of interstellar grains results in approximately a factor-of-2 increase in the temperature.

$\text{cm}^{-3}$  and  $T = 6,880$  K. The Si IV and C IV column densities predicted by all the models in Table 6 agree with the observations to better than 5%. In addition, these models do not overpredict the column densities of N V or O VI. With the exception of Model 3, the predicted Al III/Fe III ratio does not match the observations because the IVC absorption is blended with the Perseus Arm absorption. However, the predicted C IV/Al III and C IV/Fe III ratios are in agreement with the lower limits obtained from the observations, therefore our models do not overproduce either Al III or Fe III. It is important to note that the values quoted for C IV/Al III and C IV/Fe III assume that Fe and Al are depleted heavily in the models using the depleted abundances of the WNM.

Models 1, 2, and 4 result in  $P/k \leq 340$  K  $\text{cm}^{-3}$ , significantly lower than the average pressure for interstellar clouds  $P/k \sim 2500$  K  $\text{cm}^{-3}$  (Jenkins & Tripp 2001). Lower pressures are not unexpected because models of  $nT$  for warm neutral cloud halos (Andersson & Wannier 1993) predict  $nT < 1000$  K  $\text{cm}^{-3}$  at the height of Per OB1 above the Galactic plane. We note that the X-ray flux could be stronger in this active region of the Galaxy than in the solar neighborhood. Our Model 3 investigates such an increase in the X-ray flux and results in  $P/k = 2900$  K  $\text{cm}^{-3}$ , as expected from Jenkins & Tripp (2001). Model 3 also yields a temperature which is in agreement with that observed for the IVC. Note: increasing the density in Model 2 to  $\log(n_{\text{H}}) = -2.2$   $\text{cm}^{-3}$  and  $N(\text{H}_{\text{tot}}) = 20.4$   $\text{cm}^{-2}$  without increasing the radiation field results in a significantly lower C IV/Si IV = 2.0 for the observed  $N(\text{C IV})$ .

There is excellent agreement between our hot plasma photoionization models and the observations of the IVC toward HD 14434. Thus, emission of ionizing radiation by cooling hot gas is likely to be the source of the ionization in this cloud. The cooling radiation hypothesized as the ionization source in these models could arise from a general diffuse hot-ionized medium or from the super-heated interior of a supershell in the Perseus Arm (e.g., GS139-03-69).

Given the similarity of the C IV/Si IV ratio in this IVC to the Galactic average, an extension of our results implies that much of the Galactic C IV and Si IV absorption could arise as a result of photoionization by cooling radiation from a hot, thermal plasma. We note that Fox et al. (2003) have identified narrow (warm) components in C IV and Si IV toward the star HD 116852, suggesting that such absorption is not uncommon in the Galaxy (although their C IV/Si IV ratio was significantly lower than that seen toward HD 14434). Further analyses of high-resolution observations of the highly-ionized ISM are needed to determine if this phenomenon is common throughout the Galaxy.

## 6. Summary

Our STIS observations of HD 14434 reveal an IVC detected in C IV and Si IV and possibly in Fe III and Al III (Savage, Meade, & Sembach 2001). The intermediate-velocity Si IV and C IV absorption toward HD 14434 is contained in a single velocity component at a temperature of  $10,450 \pm 3,400$  K and with a non-thermal dispersion of  $12.0 \pm 0.2$  km s<sup>-1</sup>, similar to the values found for Galactic H II regions. The observed high-ion column densities are  $\log[N(\text{Si IV})] = 13.34 \pm 0.02$  cm<sup>-2</sup> and  $\log[N(\text{C IV})] = 13.92 \pm 0.02$  cm<sup>-2</sup>, which yield a C IV/Si IV ratio of  $3.8 \pm 0.3$  that is remarkably similar to the Galactic average of  $4.3 \pm 1.9$  (Sembach, Savage, & Tripp 1997).

The presence of Fe III, Al III, Si IV and C IV in low-temperature ( $10^4$  K) gas suggests that these species are in a region dominated by photoionization. The lack of significant N V and O VI absorption also support photoionization as the source of the highly-ionized IVC. Our photoionization model utilizing emission from a diffuse hot plasma is in excellent agreement with our observations indicating that this is the origin of the IVC toward HD 14434. In addition, the similarity of our C IV/Si IV ratio with the Galactic average suggests that much of the Si IV and C IV detected in the ISM could be produced from ionizing photons from a cooling hot gas.

We would like to thank the dedicated *FUSE* mission planners for their efforts in planning these observations. This work is based on data obtained for the Guaranteed Time Team by the NASA-CNES-CSA *FUSE* mission operated by the Johns Hopkins University. Financial support to U.S. participants has been provided by NASA contract NAS5-32985. The Wisconsin H-Alpha Mapper is funded by the National Science Foundation. This research made use of the Simbad database, operated at CDS, Strasbourg, France.

## REFERENCES

- Anders, E., & Grevesse, N. 1989, *Geochim. Cosmochim. Acta*, 53, 197
- Andersson, B-G, & Wannier, P. G. 1993, *ApJ*, 402, 585
- Ballet, J., Arnaud, M., Rothenflug, R. 1986, *A&A*, 161, 12
- Black, J. H. 1987, in “Interstellar Processes,” Eds. D.J. Hollenbach, & H.A. Thronson, (Dordrecht: Reidel), p. 731
- Böhringer, H., & Hartquist, T. W. 1987, *MNRAS*, 228, 915

- Borkowski, K. J., Balbus, S. A., Fristrom, C. C. 1990, ApJ, 355, 501
- Breitschwerdt, D., & Schmutzler, T. 1994, Nature, 371, 774
- Cappa, C. E., & Herbstmeier, U. 2000, AJ, 120, 1963
- Cassinelli, J. P., Waldron, W. L., Sanders, W. T., Harnden, F. R., Rosner, R., & Vaiana, G. S. 1981, ApJ, 250, 677
- Castor, J., McCray, R., & Weaver, R. 1975, ApJ, 200, L107
- Chu, Y-U. 1982, ApJ, 254, 578
- Cox, D. P., & Smith, B. W., 1974, ApJ, 189 L105
- Dixon, W. V., Kruk, J. W., & Murphy, E. M. 2001, “CalFUSE Pipeline Reference Guide”
- Edgar, R.J., & Chevalier, R.A. 1986, ApJ, 310, L27
- Ferland, G. J. 1996, Hazy: A Brief Introduction to Cloudy 1990, Univ. Kentucky Dept. Phys. Astron. Int. Rep.
- Ferland, G. J., Korista, K. T., Verner, D. A., Ferguson, J. W., Kingdon, J. B., & Verner, E. M. 1998, PASP, 110, 761
- Fox, A. J., Savage, B. D., Sembach, K. R., Fabian, D., Richter, P., Meyer, D. M., Lauroesch, J., Howk, J. C. 2003, ApJ, 582, 793
- Garmany, C.D., & Stencel, R.E. 1992, A&AS, 94, 211
- Haffner, L. M., Reynolds, R. J., Madsen, G. J., Tufte, S. L., Jaehnig, K. P., Percival, J. P., & Hausen, N. R., 2001, BAAS, 33, 1398
- Hartmann, D., & Burton, W. B. 1997, *Atlas of Galactic Neutral Hydrogen* (Cambridge, Cambridge University Press), 46
- Heiles, C. 1979, ApJ, 229, 533
- Howarth, I.D., & Prinja, R.K. 1989, ApJS, 69, 527
- Howk, J.C., & Savage, B.D. 1999, ApJ, 517, 746
- Howk, J.C., Sembach, K.R., Roth, K.C., & Kruk, J.W. 2000, ApJ, 544, 867
- Kafatos, M. 1973, ApJ, 182, 433

- Kimble et al. 1998, ApJ, 492, L83
- Knee, L. B. G., & Brunt, C. M. 2001, Nature, 412, 308
- Lemoine et al. 2002, ApJS, 140, 67
- Lindler, D., & Bowers, C. 2000, BAAS, 32, 1418
- Lozinskaya, T. A. 1991, in IAU Symp. 143, Wolf-Rayet Stars and Interrelations with Other Massive Stars in Galaxies, ed. K. A. van der Hucht & B. Hidayat (Dordrecht: Kluwer), 365
- Lupton, R. 1993, *Statistics in Theory and Practice*, (Princeton, Princeton University Press), 100
- Madsen, G.J., Haffner, L.M., & Reynolds, R.J. 2002, astro-ph/0112232
- Marco, A., & Bernabeu, G. 2001, A&A, 372, 477
- McKee, C. F., & Ostriker, J. P. 1977, ApJ, 218, 148
- McLachlan, A., & Nandy, K. 1985, MNRAS, 215, 473
- Moos et al. 2000, ApJ, 538, L1
- Morton, D. C. 1991, ApJS, 77, 119
- Morton, D. C., York, D. G., & Jenkins, E. B. 1986, ApJ, 302, 272
- Normandeau, M., Taylor, A.R., & Dewdney, P.E. 1996, Nature, 380, 687
- Phillips, A. P., & Gondhalekar, P. M. 1981, MNRAS, 196, 533
- Reynolds, R. J. 1991, in IAU Symp. 144, The Interstellar Disk-Halo Connection in Galaxies, ed. H. Bloemen (Dordrecht: Kluwer), 67
- Reynolds, R. J., Sterling, N. C., & Haffner, L. M. 2001, ApJ, 558, 101
- Rogerson, J. B., York, D. G., Drake, J. F., Jenkins, E. B., Morton, D. C., & Spitzer, L. 1973, ApJ, 181, L110
- Sahnou et al. 2000, ApJ, 538, L7
- Savage, B. D., Meade, M. R., & Sembach, K. R. 2001, ApJS, 136, 631
- Savage, B. D., & Sembach, K. R., 1991, ApJ, 379, 245

- Savage, B. D., Sembach, K. R., & Lu, L. 1997, *AJ*, 113, 2158
- Savage, B.D., et al. 2002, *ApJS*, submitted
- Schild, R. 1967, *ApJ*, 148, 449
- Sembach, K. R. 1999, in *Stromlo Workshop on High-Velocity Clouds*, eds. Gibson, B. K., & Putman, M. E., *ASP Conference Series Vol. 166*, 243
- Sembach, K. R., Howk, J. C., Ryans, R. S. I., Keenan, F. P., 2000, *ApJ*, 528, 310
- Sembach, K.R., & Savage, B.D. 1992, *ApJS*, 83, 147
- Sembach, K.R., Savage, B.D., & Tripp, T.M. 1997, *ApJ*, 480, 216
- Shapiro, P. R., & Benjamin, R. A. 1992, *PASP*, 103, 923
- Shapiro, P. R., & Moore, R. T. 1976, *ApJ*, 207, 460
- Slavin, J. D., & Frisch, P. C. 2002, *ApJ*, 565, 364
- Slavin, J. D., Shull, J. M., & Begelman, M. C. 1993, *ApJ*, 407, 83
- Sofia, U. J., Fabian, D., & Howk, J. C. 2000, *ApJ*, 531, 384
- Spitzer, L. 1996, *ApJ*, 458, L29
- Sutherland, R. S., & Dopita, M. A. 1993, *ApJS*, 88, 253
- Walborn, N. R. 1972, *AJ*, 77, 312
- Weaver, R., McCray, R., Castor, J., Shapiro, P., & Moore, R. 1977, *ApJ*, 218, 377
- Williamson, F. O., Sanders, W. T., Kraushaar, W. L., McCammon, D., Borken, R., & Bunner, A. N. 1974, *ApJ*, 193, L133
- Woodgate et al. 1998, *PASP*, 110, 1183

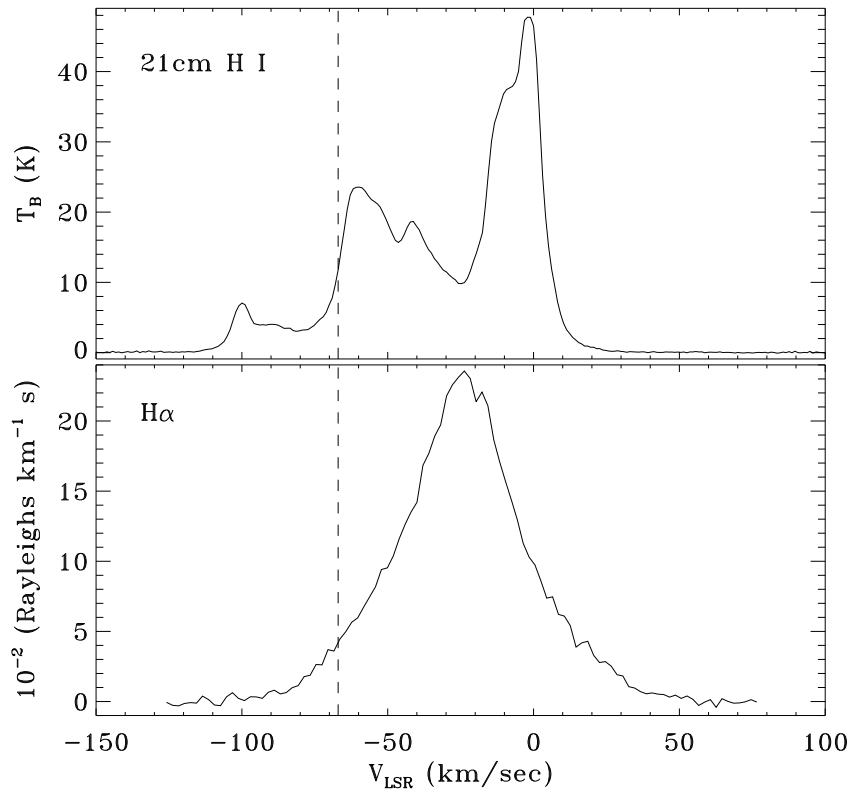


Fig. 1.— 21cm H I emission (Hartmann & Burton 1997) and H $\alpha$  WHAM data (Haffner et al. 2001) toward HD 14434 are presented. The H I data clearly reveal two components from the Local ( $V_{lsr} \sim 0$  km s $^{-1}$ ) and Perseus Arms ( $V_{lsr} \sim -50$  km s $^{-1}$ ) and a single weak component associated with the Outer Arm ( $V_{lsr} = -100$  km s $^{-1}$ ). The H $\alpha$  data show a single broad component centered at  $V_{lsr} = -25$  km s $^{-1}$ . The vertical line is at  $V_{lsr} = -67$  km s $^{-1}$ , the velocity of the IVC. Neither H I nor H $\alpha$  reveal any clues as to the presence of the IVC at  $V_{lsr} = -67$  km s $^{-1}$ .

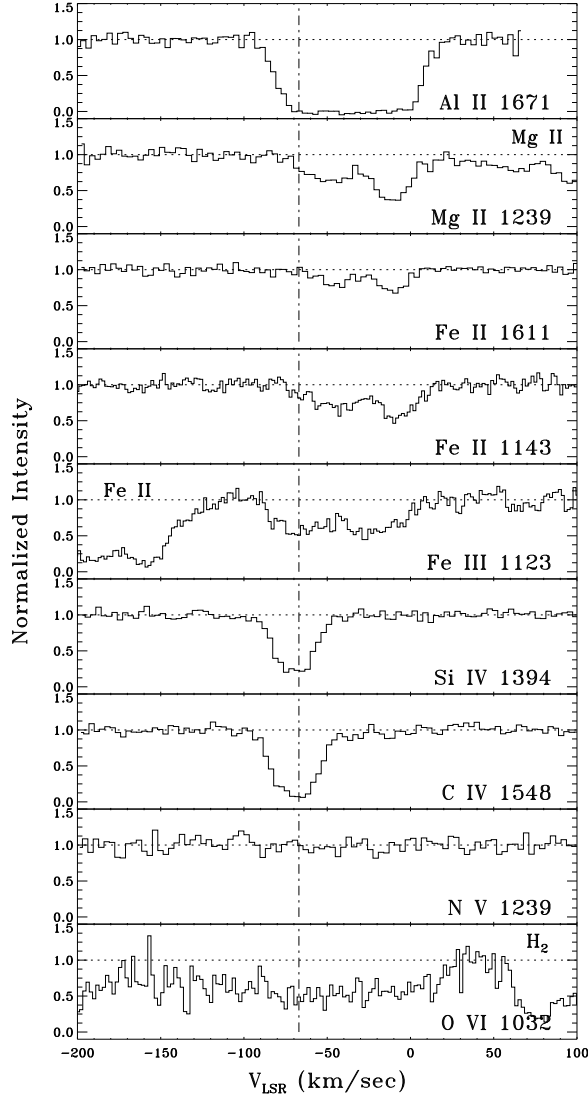


Fig. 2.— Low and high-ionization absorption along the line of sight toward HD 14434 are presented. The Fe II  $\lambda$ 1143, Fe III  $\lambda$ 1123, and O VI  $\lambda$ 1032 are *FUSE* data while the remaining spectra were obtained with STIS. The flux is normalized to unity and is represented by the dotted line. The dashed-dotted line at  $-67 \text{ km s}^{-1}$  represents the central velocity of the high-velocity highly-ionized gas. The spectrum containing Al II  $\lambda$ 1671 has a cut-off at  $70 \text{ km s}^{-1}$  because it is at the edge of an echelle order on the STIS detector. Interstellar C II, C III, Si II, and Si III show similar absorption profiles to Al II. The broad absorption in the O VI spectrum is attributed to a stellar wind feature (see text for details).

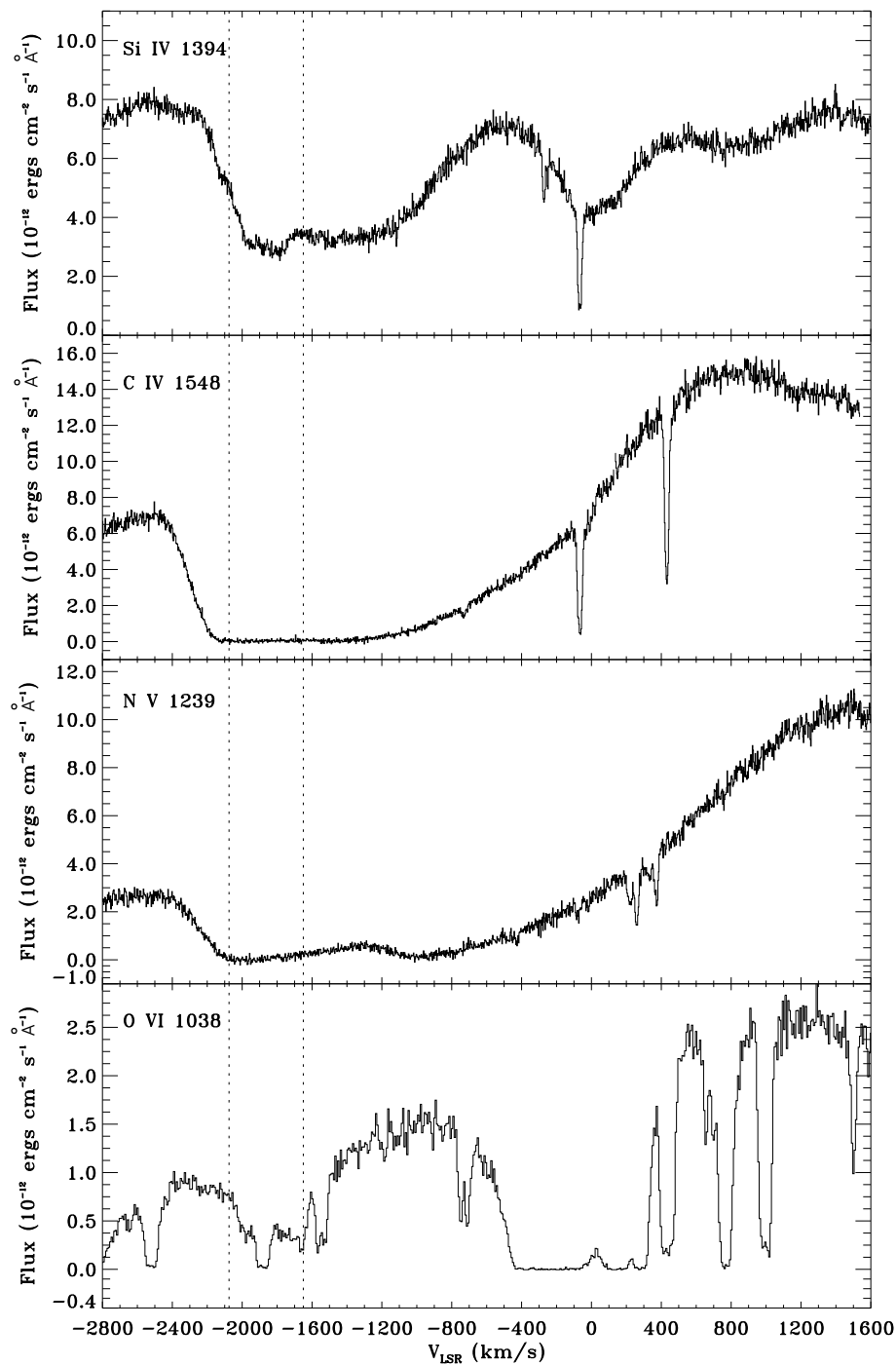


Fig. 3.— The wind line profiles of the following species are shown: Si IV, C IV, N V, and O VI. There is an obvious wind feature evident in the Si IV wind profile. The dotted lines show the velocity range over which the feature is present ( $\Delta v \sim 400 \text{ km s}^{-1}$ ). The broad absorption feature in the O VI spectrum (bottom panel) is attributed to the stellar wind feature (see text for details).

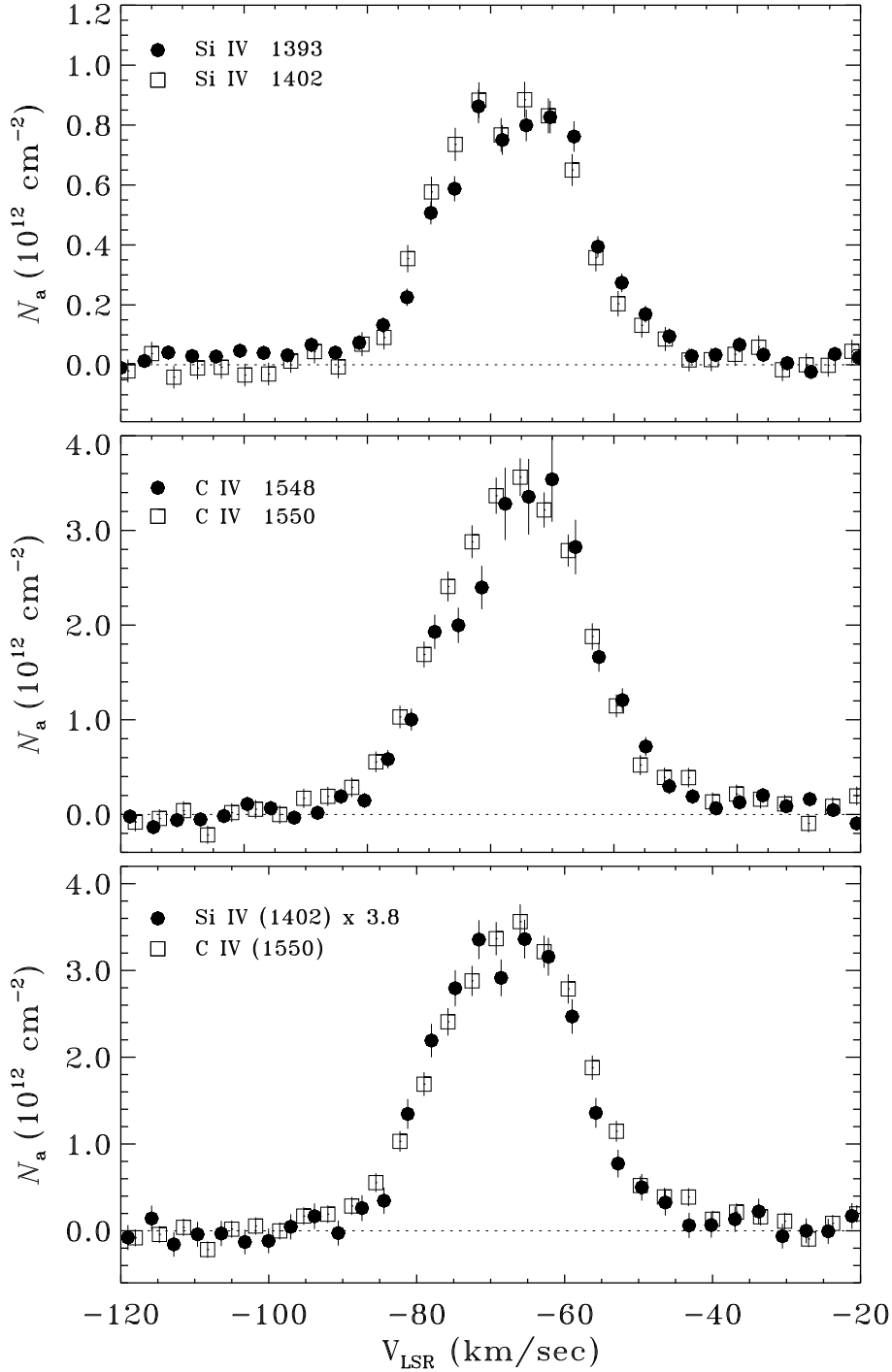


Fig. 4.— *Upper panel:* — Apparent column density profiles of the Si IV 1393 and 1402 Å lines. The solid circles represent the stronger member of the doublet, while the open squares denotes the weaker line. *Middle panel:* — Apparent column densities of the C IV doublet  $\lambda\lambda$  1548, 1550. The symbols are the same as for the top panel. *Bottom panel:*— Apparent column densities of the weaker members of the Si IV and C IV doublets and reveals that a C IV/Si IV ratio of 3.8 is representative over the entire velocity range. The overlap of both species suggests that they are co-spatial. There is excellent agreement in the  $N_a(v)$  of both members of the Si IV and C IV doublets indicating little or no evidence of saturation.

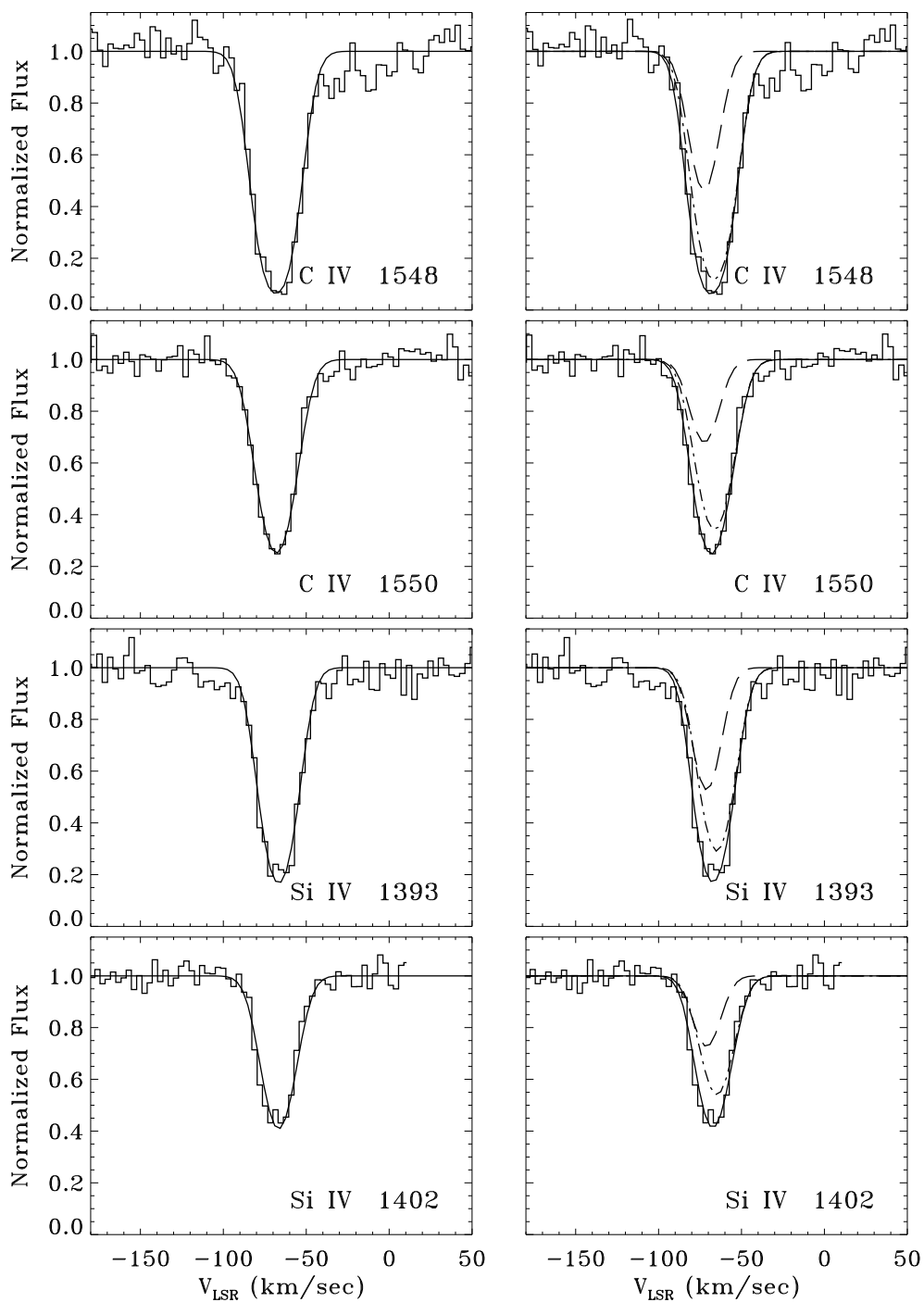


Fig. 5.— The left panels show the one-component model fits to the Si IV and C IV doublets. The right side shows the two-component model fits. There is only a 30% confidence in the second component.

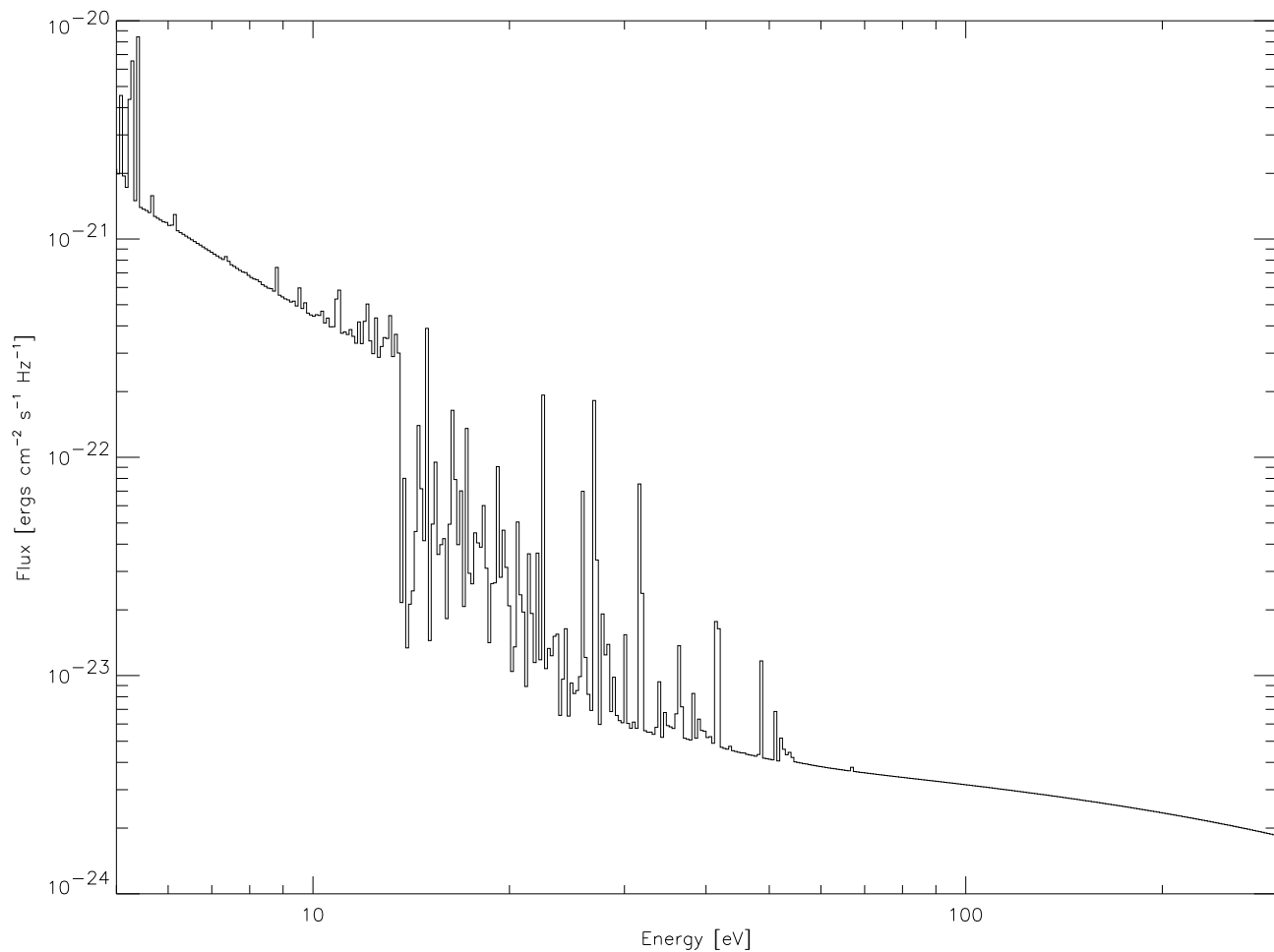


Fig. 6.— The ionizing spectrum from cooling hot diffuse gas that was used to calculate Models 1 and 2 in Table 6 is shown. This spectrum includes the diffuse interstellar radiation field (Black 1987) and emission from a thermal plasma at  $\log(T_{\text{plasma}}) = 6.1$  K whose flux was normalized to the observed diffuse X-ray background for the Local Bubble.

Table 1. Adopted Stellar Parameters for HD 14434

Quantity	Value	Source
Spectral Type	O5.5 Vnfp	Walborn (1972)
$V$ [mag]	8.49	Simbad <sup>a</sup>
$E(B - V)$ [mag]	0.48	Diplas & Savage (1994)
$(l, b)$	(135°1, -3°8)	Simbad <sup>a</sup>
$T_{eff}$ [K]	44,000	Howarth & Prinja (1989)
$\log(L_*/L_\odot)$	5.4	Howarth & Prinja (1989)
$V_\infty$ [km s <sup>-1</sup> ]	2,120	This work
$d$ [kpc]	2.3	Diplas & Savage (1994)
$z$ [pc]	-153	Diplas & Savage (1994)
$N(\text{H I})$ [cm <sup>-2</sup> ]	$(2.82 \pm 1.21) \times 10^{21}$	Diplas & Savage (1994)

<sup>a</sup>The Simbad database is operated at CDS, Strasbourg, FR.

Table 2. Ions toward HD 14434

Species	IP <sup>a</sup> [eV]	$\lambda_o$ <sup>b</sup> [Å]	$\log(\lambda f)$ <sup>b</sup> [Å]	$V_{LSR}$ [km s <sup>-1</sup> ]	$W_\lambda$ <sup>c</sup> [mÅ]	$\log(N_a)$ <sup>d</sup> [cm <sup>-2</sup> ]
Mg II	7.7–15.0	1239.925	0.190 <sup>e</sup>	-47.1 ± 1.1	43.1 ± 3.7	15.77 ± 0.04
		1240.395	-0.110 <sup>e</sup>	-48.1 ± 2.2	19.9 ± 3.8	15.67 ± 0.09
Fe II	7.9–16.2	1121.975	1.351 <sup>f</sup>	-46.2 ± 0.9	140.6 ± 5.0	15.05 ± 0.03
		1127.098	0.483 <sup>f</sup>	-41.8 ± 1.5	23.7 ± 2.8	14.97 ± 0.06
		1611.201	0.339	-42.5 ± 1.3	24.8 ± 3.3	14.98 ± 0.06
Al III <sup>g</sup>	18.8–28.5	1854.716	3.017	-50.1 ± 4.2	166 ± 17	13.05 ± 0.05
		1862.790	2.716	-68.5 ± 6.4	76 ± 15	13.01 ± 0.10
Fe III	16.2–30.7	1122.546	2.260	-61.7 ± 0.9	58.1 ± 3.9	13.61 ± 0.04
Si IV	33.5–45.1	1393.755	2.855	-66.6 ± 0.4	110.3 ± 3.0	13.32 ± 0.02
		1402.770	2.554	-67.5 ± 0.5	72.5 ± 2.3	13.35 ± 0.02
C IV	47.9–64.5	1548.195	2.470	-65.7 ± 0.5	151.0 ± 4.8	13.89 ± 0.04
		1550.770	2.169	-66.5 ± 0.5	114.8 ± 3.8	13.93 ± 0.02
N V	77.5–97.9	1238.821	2.289	...	≤ 10.6	≤ 12.72 <sup>h</sup>
		1242.804	1.988	...	≤ 4.7	≤ 12.65 <sup>h</sup>
O VI	113.9–138.1	1031.926	2.137	...	≤ 54.4 <sup>i</sup>	≤ 13.78 <sup>h</sup>

<sup>a</sup>Creation and destruction ionization potentials (Lang 1980).

<sup>b</sup>Morton (1991).

<sup>c</sup>1- $\sigma$   $W_\lambda$  uncertainties and upper limits derived following the prescription in Morton, York, & Jenkins (1986).

<sup>d</sup> $N$  derived from the apparent optical depth method (Sembach & Savage 1992).

<sup>e</sup>Oscillator strengths from Sofia, Fabian, & Howk (2000).

<sup>f</sup>Howk et al. (2000).

<sup>g</sup>Savage, Meade, & Sembach (2001) – based on high-resolution ( $R \sim 25 \text{ km s}^{-1}$ ) *IUE* observations.

<sup>h</sup>3- $\sigma$  upper limit assuming a  $b$ -value of  $12.3 \text{ km s}^{-1}$  derived from C IV and Si IV results.

<sup>i</sup>O VI upper limit includes absorption by a possible stellar wind feature (see text).

Table 3. Profile Synthesis Results for Si IV and C IV

$V_{LSR}$ [km s <sup>-1</sup> ]	$\log[N(\text{Si IV})]$ [cm <sup>-2</sup> ]	$\log[N(\text{C IV})]$ [cm <sup>-2</sup> ]	$\frac{N(\text{C IV})}{N(\text{Si IV})}$	$v_{\text{nt}}^{\text{a}}$ [km s <sup>-1</sup> ]	$T$ [K]	$\chi^2/\nu$
One Component Model						
$-67.3 \pm 0.1^{\text{b}}$	$13.35 \pm 0.01$	$13.93 \pm 0.01$	$3.8 \pm 0.1$	$12.0 \pm 0.2$	$10,450 \pm 3,400$	1.42
Two Component Model <sup>b</sup>						
-65.8	13.16	13.81	4.4	10.7	26,500	1.43
-71.2	12.89	13.31	2.6	11.3	10,100	

<sup>a</sup>Non thermal velocity.

<sup>b</sup>1- $\sigma$  errors do not include continuum placement uncertainties. No errors are reported for the two component model due to the low confidence in the second component.

Table 4. Adopted Parameters of IVC Absorption

Species	$b$ -value [km s <sup>-1</sup> ]	$V_{LSR}$ [km s <sup>-1</sup> ]	$\log(N)^a$ [cm <sup>-2</sup> ]
Mg II	...	-47.1 ± 1.1	15.75 ± 0.04
Fe II	23.0 ± 4.4	-46.2 ± 0.9	14.90 ± 0.06 <sup>b</sup>
Al III <sup>c,d</sup>	...	-56.3 ± 3.3	13.04 ± 0.05
Fe III <sup>d</sup>	...	-61.7 ± 0.9	13.61 ± 0.04
Si IV	12.3 ± 0.3	-66.6 ± 0.4	13.34 ± 0.02
C IV	12.6 ± 0.3	-65.7 ± 0.5	13.92 ± 0.02
N V	...	...	≤ 12.65 <sup>e</sup>
O VI	...	...	≤ 13.73 <sup>e,f</sup>

<sup>a</sup>Weighted average of  $N_a(v)$  from Table 2.

<sup>b</sup>Derived from curve of growth (see text for details).

<sup>c</sup>Savage, Meade, & Sembach (2001).

<sup>d</sup>Contains contribution from both IVC and Perseus Arm material.

<sup>e</sup>Upper limit to  $N$  determined with an assumed  $b$ -value of 12.3 km s<sup>-1</sup> derived from average C IV and Si IV results.

<sup>f</sup>O VI upper limit includes effect of possible stellar wind feature (see text).

Table 5. H II Region Photoionization Models<sup>a</sup>

Model	$\log n_{\text{H}}$ [cm <sup>-3</sup> ]	$\log U^{\text{b}}$	$\log[N(\text{C IV})]$ [cm <sup>-2</sup> ]	$\frac{N(\text{C IV})}{N(\text{Si IV})}$	$\frac{N(\text{Al III})}{N(\text{Fe III})}$
1	-4.0	1.3	8.0	0.79	0.05
2	-2.0	-0.7	8.6	0.77	0.06
3	0.0	-2.7	10.3	0.43	0.04

<sup>a</sup>All column densities assume abundances appropriate for the WNM following Sembach et al. (2000).

<sup>b</sup>The ionization parameter: the dimensionless ratio of photon to particle densities.

Table 6. Hot Plasma Models

Quantity	Observed	1	2	3 <sup>b</sup>	4
Abundances <sup>a</sup>	...	Solar	WNM	WNM	WNM
$\log(T_{\text{plasma}})$ [K]	...	6.1	6.1	6.1	7.0
$\log(n_{\text{H}})$ [cm <sup>-3</sup> ]	...	-2.9	-2.8	-1.8	-0.7
$\log(U)$	...	-1.6	-1.7	-2.9	-1.7
$\log[N(\text{H}_{\text{tot}})]$ [cm <sup>-2</sup> ]	...	18.55	19.01	18.92	18.99
$T$ [K]	10,450 ± 3,400	4,630	6,930	10,100	6,880
$\log[N(\text{C IV})]$ [cm <sup>-2</sup> ]	13.92 ± 0.02	13.92	13.92	13.92	13.92
$\frac{N(\text{C IV})}{N(\text{Si IV})}$	3.8 ± 0.3	3.8	3.8	3.7	3.8
$\frac{N(\text{C IV})}{N(\text{N V})}$	≥ 18.6	194	180	89	171
$\frac{N(\text{C IV})}{N(\text{O VI})}$	≥ 1.6	6341	9749	1475	8165
$\frac{N(\text{C IV})}{N(\text{Al III})}$	≥ 7.6	18	126	331	138
$\frac{N(\text{C IV})}{N(\text{Fe III})}$	≥ 2.0	25	139	49	163
$\frac{N(\text{Al III})}{N(\text{Fe III})}$	0.3 ± 0.1 <sup>c</sup>	1.4	1.1	0.2	1.2

<sup>a</sup>Assumed to be Solar or depleted abundances found for the WNM (see text). Solar abundances use Anders & Grevesse (1989) summary with the oxygen abundance of Holweger (2001) and do not include interstellar grains. The WNM abundances adopt the relative abundances summarized in Sembach et al. (2000) and includes interstellar grains.

<sup>b</sup>Uses X-ray flux a factor-of-10 higher than observed in the Local Bubble used to compute models 1 and 2 (see Figure 6).

<sup>c</sup>Contains contribution from both IVC and Perseus Arm gas because both components are blended together.